Quantum study of vibrational excitation in the threedimensional collisions of CO2 with rare gas atoms

D. C. Clary

Citation: The Journal of Chemical Physics **75**, 209 (1981); doi: 10.1063/1.441827
View online: http://dx.doi.org/10.1063/1.441827
View Table of Contents: http://scitation.aip.org/content/aip/journal/jcp/75/1?ver=pdfcov
Published by the AIP Publishing

Quantum study of vibrational excitation in the three-dimensional collisions of CO_2 with rare gas atoms

D. C. Clary[a)]

Department of Chemistry, University of Manchester, Manchester M13 9PL, United Kingdom
(Received 28 May 1980; accepted 20 June 1980)

A combined vibrational close-coupling and rotational infinite order sudden technique is described for calculating vibrational excitation cross sections $\sigma_{vv'}$ for the three-dimensional collisions of atoms with linear triatomic molecules. The method treats anharmonic, Coriolis, and vibrational angular momentum terms in the molecular Hamiltonian accurately, and is applicable to any realistic potential energy surface expressed in numerical or functional form. Application of the method to X–$CO_2(v_1v_2^{l}v_3)$ collisions, where X=He, Ne, or Ar, is described. An accurate anharmonic CO_2 potential, expressed in terms of bond and angle displacements, is employed. The X–CO_2 interaction potentials are more approximate and are expanded in terms of atom–atom pair potentials. Calculations of $\sigma_{vv'}$, over a grid of energies sufficient to give rate coefficients $k_{vv'}$ for transitions between the low-lying states of CO_2 for temperatures up to 300 K, have been performed. Propensities for particular collisional excitations involving the symmetric stretch, bending, and asymmetric stretch vibrational modes of CO_2 are examined. It is found that the magnitudes of the $\sigma_{vv'}$ are largely determined by the energy differences between the v and v' levels. For example, excitation of the ground (00^00) state to the first excited bending state (01^10) is found to be favored. $\sigma_{vv'}$ for near resonant transitions such as $(02^00)\rightarrow(02^20)$ are found to increase with increasing mass of X. Deactivation of the (00^01) state to the (11^10) state is favored over other transitions. The ratios of the deactivation cross section for the level (00^01) to the deactivation cross sections for lower levels such as (01^10) are small, although these ratios do increase with increasing mass of X, in agreement with experimental findings. Comparison of calculated $k_{vv'}$, for deactivation of the (01^10) level, with those obtained in recent photoacoustic experiments is quite encouraging, considering the approximate nature of the X–CO_2 interaction potentials used. For X=He and Ne these calculated $k_{vv'}$ are within a factor of 5 of the experimental results and have the correct temperature dependence, while for X=Ar the calculations are much larger than the experimental results, and the temperature dependence is too shallow. The computer program used in the calculations is automatic and general, and should be applicable to many other atom–linear triatomic molecule collisions.

I. INTRODUCTION

The excitation of the vibrational energy levels of triatomic molecules by collisions with atoms has been studied in ultrasonic wave,[1] shock tube,[2] photoacoustic,[3] molecular beam,[4] and laser-induced fluorescence experiments.[5–7] To complement these experiments, reliable quantum-dynamical theories are required. In this paper a description is given of the application of a combined vibrational close-coupling and rotational infinite order sudden (VCC–IOS) method to the three dimensional (3D) collisions of atoms with linear triatomic molecules. Vibrational excitation cross sections for the process

$$CO_2(v_1v_2^{l}v_3) + X \rightarrow CO_2(v_1'v_2'^{l'}v_3') + X \qquad (I)$$

are reported, where X is a rare gas atom (He, Ne, or Ar). v_1, v_2^{l}, and v_3 are the quantum numbers of the symmetric stretch, bending and asymmetric stretch vibrational modes of CO_2, respectively. Calculated rate coefficients for the collisional deactivation of CO_2 (01^10) are compared with those obtained in recent photoacoustic experiments.[3]

The theoretical study of vibrational excitation in CO_2–rare gas collisions is not only useful for interpreting experiments such as those mentioned above but is also important for providing an understanding of the factors affecting the power of CO_2 lasers,[8,9] which are strongly influenced by the collisional deactivation of certain CO_2 vibrational levels by rare gas atoms.[5,6,8] For example, the strong 9.4 and 10.6 μm CO_2 laser transitions[8] occur between the (00^01) level and the two levels in Fermi resonance (02^00) and (10^00), while the 16 and 14 μm laser transitions[10] occur between these latter two levels and the (01^10) level. Accurate values of collisional deactivation rate coefficients for levels such as these are required for the computer simulation of the CO_2 lasers.[11]

The IOS method (for recent reviews see Refs. 12 and 13) has previously been shown to give reliable rotational excitation cross sections for the collisions of rare gas atoms with CO_2 treated as a rigid rotor.[14–16] Many calculations of rotational excitation cross sections for atom–diatom collisions have shown[12–15] that the IOS technique is most reliable when the rotational energy spacings are very small compared to the collisional energy. For CO_2 in its ground vibrational state, the rotational energy level spacing for the most probable rotational level at room temperature ($j=16$) is only 1.5 meV.[17]

The VCC–IOS method has been applied previously[18,19] to the study of vibrational–rotational excitation in atom–diatom collisions. In this technique it is necessary to solve the vibrational close-coupling equations over a grid of fixed atom–molecule scattering angles. Since the vibrational part of the close-coupling equations is treated accurately in the VCC–IOS technique, the method should yield accurate vibrational excitation cross sections under those conditions for which the IOS method

a)Present address: Department of Chemistry, University of Manchester Institute of Science and Technology, Manchester M60 1QD, United Kingdom.

 0021-9606/81/130209-11$01.00

itself is reliable for rotational excitation.[18–20] This has been borne out in comparisons with accurate calculations of vibrational excitation cross sections in atom–diatom collisions.[18,19] Since the IOS method works well for rare gas–rigid rotor CO_2 collisions, the VCC–IOS method is expected to work well for rare gas–vibrating CO_2 collisions. This work presents, to our knowledge, the first application of the VCC–IOS technique to the study of vibrational excitation in atom–triatomic molecule collisions.

Several recent studies of vibrational energy transfer in atom–linear triatomic collisions in one dimension have been reported.[21–26] These have included quantum,[21–24] semiclassical,[25] and quasiclassical studies.[26] Classical trajectory calculations on vibrational excitation in CO_2–rare gas collisions have been carried out in two[27] and three[28] dimensions. A classical trajectory study of the deactivation of the bending mode of CO_2 by H_2 has also been reported,[29] as have classical trajectory calculations on some atom–vibrating nonlinear triatomic collisions.[30] The sudden approximation has been incorporated into the quasiclassical method[31] and this technique has been used to compute quasiclassical vibrational excitation cross sections for $Li^+ + CO_2$ collisions.[32] A particular feature of these quasiclassical studies[28–32] is that Coriolis and anharmonic terms in the CO_2 Hamiltonian, which couple different vibrational modes together, cause difficulties in the assignment of quantum numbers to individual trajectories. These coupling terms cause no difficulties in the present quantum treatment.

A recent semiclassical study of vibrational excitation of CO_2 by Ne in 3D has been made by Billing.[33] Most previous quantum treatments of atom–vibrating triatomic molecule collisions in 3D have made use of first order perturbation methods.[3,5,34] A recent study of Li^+–vibrating CO_2 collisions has been made, however, using a many-body approximation.[35]

In Sec. II the VCC–IOS method as applied to general atom–vibrating linear triatomic systems is described in detail. These systems cause several extra computational problems to those met in atom–diatom collisions.[18,19] In particular, four different vibrational modes have to be dealt with instead of just one. A significant aspect of the method described here is that the vibrational close-coupling matrix elements are evaluated using accurate numerical, as opposed to analytical, techniques. The method is therefore readily applicable to any realistic atom–linear triatomic potential energy surface in numerical or functional form. Coriolis, anharmonic, and vibrational angular momentum terms in the molecular Hamiltonian are also treated accurately.

In Sec. III extensive calculations of vibrational excitation cross sections and rate coefficients for process I are reported and discussed. A comparison of calculated rate coefficients for the collisional deactivation of CO_2 (01^10) with experimental results is also made.[3] The CO_2 potential used in the calculations is of a realistic anharmonic form expressed in terms of bond and angle displacements, the parameters in the potential being determined from spectroscopic measurements. The X–CO_2 interaction potentials are much more approximate, and are of a form used previously in quasiclassical calculations.[28] They are expressed as a sum of atom–atom potentials, which are determined from molecular beam scattering and virial coefficient data on the X–Ne systems.[36,37] In Sec. IV a summary of the main conclusions of this work is presented.

II. THEORY

A. Coordinates and Hamiltonians

The Hamiltonian for a linear triatomic molecule ABC can be written[38,39] as

$$H_{ABC} = H^V_{ABC} + H^{V-R}_{ABC} + H^R_{ABC} \ . \tag{1}$$

H^{V-R}_{ABC} and H^R_{ABC} contain vibrational–rotational and rotational kinetic energy terms, respectively,

$$H^V_{ABC} = \sum_{k=1}^{4} \tfrac{1}{2} P_k^2 + H_{cor} + V_{ABC}(Q_1, Q_{2a}, Q_{2b}, Q_3) \tag{2}$$

and

$$H_{cor} = (1/2I')(\pi_x^2 + \pi_y^2) \ , \tag{3}$$

where

$$\pi_\alpha = \sum_{kl} \epsilon^\alpha_{kl} Q_k P_l \ . \tag{4}$$

I' is very closely related to the moment of inertia of ABC.[38,39] ϵ^α_{kl} are Coriolis coupling coefficients.[38] Q_1, Q_{2a}, Q_{2b}, and Q_3 are the symmetric stretch, two bending modes, and asymmetric stretch normal coordinates of ABC, respectively. The $\{P_k\}$ are the corresponding momenta. V_{ABC} is the molecular potential.

The origin of the coordinates for the molecule is defined by

$$\sum_i m_i \mathbf{r}_i = \mathbf{0} \tag{5}$$

and the molecule-fixed axes are defined by

$$\sum_i m_i \mathbf{r}_i^0 \times \mathbf{r}_i = \mathbf{0} \ , \tag{6}$$

where m_i, $\mathbf{r}_i$, and $\mathbf{r}_i^0$ are the mass, distance vector and equilibrium position of atom i, respectively.

The normal coordinates are related to the molecule fixed Cartesian coordinates $[x_i, y_i, z_i]$ by the linear relationship

$$U_i = U_{i1}Q_1 + U_{i2a}Q_{2a} + U_{i2b}Q_{2b} + U_{i3}Q_3 + U_{i4}, \tag{7}$$

where U_i is x_i, y_i, or z_i. The coefficients in Eq. (7) can be obtained using the FG matrix method.[38] For symmetric linear triatomics [A=C] the expansions (7) have the simple forms[40]

$$\begin{aligned} &x_1 = x_3 = -M_1 Q_{2a} \ , \quad x_2 = M_2 Q_{2a} \ , \\ &y_1 = y_3 = -M_1 Q_{2b} \ , \quad y_2 = M_2 Q_{2b} \ , \\ &z_1 = -M_1 Q_3 - M_3 Q_1 - R_e \ , \quad z_2 = M_2 Q_3 \ , \\ &z_3 = -M_1 Q_3 + M_3 Q_1 + R_e \ , \end{aligned} \tag{8}$$

where

$$M_1=(M_B/2M_CM_T)^{1/2}\ ,\quad M_2=(2M_C/M_BM_T)^{1/2}\ ,$$
$$M_3=(1/2M_C)^{1/2}\ ,\quad \text{and}\quad M_T=M_A+M_B+M_C\ . \tag{9}$$

M_A, M_B, and M_C are the masses of the atoms A, B, and C, respectively. R_e is the AB internuclear distance at equilibrium.

To determine the eigenfunctions of H^V_{ABC} it is convenient to use the transformations $Q_{2a}=Q_2\cos\delta$ and $Q_{2b}=Q_2\sin\delta$. The basis set

$$g_{\lambda p}(\delta)\prod_{j=1}^{3}Q_j^{N_j-1}\exp(-\tfrac{1}{2}t_jQ_j^2) \tag{10}$$

can then be used in solving

$$H^V_{ABC}\psi_{vp}=E_v\psi_{vp}\ . \tag{11}$$

In Eq. (10), $g_{\lambda p}(\delta)$ is of two different types:

$$g_{\lambda p=e}(\delta)=\cos\lambda\delta\quad\text{or}\quad g_{\lambda p=o}(\delta)=\sin\lambda\delta\ .$$

e stands for even and o for odd. The vibrational angular momentum quantum number $\lambda=N_2-1, N_2-3, \ldots, 1$ or 0. The $\{N_j\}$ are integers (≥ 1); t_j are the fundamental frequencies; v represents an energy level which can be labeled using the simple-harmonic oscillator notation $v=(v_1v_2^{\lambda}v_3)$; for $\lambda>0$, the levels $\psi_{vp=e}$ and $\psi_{vp=o}$ are degenerate.

H_{ABC} contains terms in χ which is an arbitrary function of the Euler angles θ and ϕ.[38] In constructing a Hamiltonian suitable for determining the eigenfunctions of H_{ABC}, Watson[39] replaced χ by the independent Euler angle χ' and derived the isomorphic Hamiltonian H_{iso}, in which H^R_{ABC} and H^{V-R}_{ABC} are replaced by

$$H'^R_{ABC}=(1/2I')[\Pi_x'^2+\Pi_y'^2] \tag{12}$$

and

$$H'^{V-R}_{ABC}=-(1/I')[\Pi_x'\pi_x+\Pi_y'\pi_y]\ . \tag{13}$$

Π_x' and Π_y' are rotational angular momentum operators.[39] Diagonalization of H_{iso} using the basis

$$\psi_{vp}D^J_{\lambda M_j}(\chi',\theta,\phi) \tag{14}$$

yields the eigenfunction ψ'_{ABC}. The exact eigenfunction ψ_{ABC} is then obtained[39] from ψ'_{ABC} by setting $\chi=\chi'$ and multiplying by $(2\pi)^{1/2}$. Note that one of the quantum numbers implied by v is λ which is also one of the quantum numbers defining the Wigner rotation function[48] $D^J_{\lambda M_j}$.

In Fig. 1 a diagram describing the X–ABC collisional system is presented with ABC having a bent nonequilibrium geometry. The polar angles of X with respect to the molecular fixed axes are θ_x and ϕ_x, respectively. R is the distance from X to the origin. The distances from atom X to atom i of ABC are

$$R_i=[(x_i-R\sin\theta_x\cos\phi_x)^2+(y_i-R\sin\theta_x\sin\phi_x)^2+(z_i-R\cos\theta_x)^2]^{1/2}\ . \tag{15}$$

Given R, θ_x, and ϕ_x, it is straightforward to relate $\{R_i\}$ to the $\{Q_i\}$ using Eqs. (7) and (15).

The Schrödinger equation for the X–ABC collisional system is

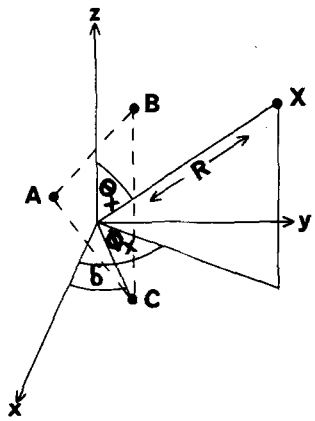

FIG. 1. Coordinates for collision of X with ABC in a bent nonequilibrium configuration.

$$H\psi=\left(-\frac{\hbar^2}{2\mu}\frac{1}{R}\frac{\partial^2}{\partial R^2}R+\frac{\mathbf{L}^2}{2\mu R^2}+H_{ABC}+V_{int}\right)\psi=E\psi\ . \tag{16}$$

L is the orbital angular momentum operator of X relative to ABC. V_{int} is the X–ABC interaction potential. μ is the reduced mass of the collisional system. $E=E_{tot}$ is the total energy.

B. VCC-IOS method

In the present VCC–IOS approximation $\mathbf{L}^2$ in Eq. (16) is replaced[51] by $\bar{l}(\bar{l}+1)\hbar^2$ and H_{ABC} is replaced by H^V_{ABC}, which is defined in Eq. (2). The total wave function is then expanded in the close-coupling form

$$\psi=\sum_{v'p'}\frac{f^{\bar{l}vp}_{v'p'}(R,\theta_x,\phi_x)\psi_{v'p'}(Q_1,Q_2,Q_3,\delta)}{R} \tag{17}$$

and substitution in (16), multiplication by $\psi_{v'p'}$, and integration over the internal coordinates yields

$$\left[\frac{d^2}{dR^2}+k^2_{v'}-\frac{\bar{l}(\bar{l}+1)}{R^2}\right]f^{\bar{l}vp}_{v'p'}(R,\theta_x,\phi_x)=\frac{2\mu}{\hbar^2}\sum_{v''p''}V^{v'p'}_{v''p''}(R,\theta_x,\phi_x)f^{\bar{l}vp}_{v''p''}(R,\theta_x,\phi_x)\ , \tag{18}$$

where

$$k^2_{v'}=(2\mu/\hbar^2)[E-E_{v'}]\ . \tag{19}$$

It follows from the expressions for R_i [given in Eq. (15)] and $\mathbf{r}_i$ [given in Eqs. (7) and (8) for symmetric ABC] that V_{int} can be expanded in the form

$$V_{int}=\sum_n h_n(R,\theta_x,Q_1,Q_2,Q_3)\cos[n(\phi_x-\delta)]\ . \tag{20}$$

For each value of ϕ_x, the linearly independent functions of the two different types $\bar{g}_{np=e}=\cos[n(\phi_x-\delta)]$ and $\bar{g}_{np=o}=\sin[n(\phi_x-\delta)]$ can be constructed and used in the molecular basis set, in place of g_{np}. The close-coupling matrix elements over V_{int} between basis functions containing $\bar{g}_{n'p'}$ and $\bar{g}_{n''p''}$ are zero for $p'\neq p''$. Furthermore, the values of these matrix elements are independent of ϕ_x for $p'=p''$. Thus the solution of the close-coupling equations (18) can be divided up into two separate groups for which $p'=p''=e$ and $p'=p''=o$. Since ϕ_x is arbitrary it can be set to zero so that $\bar{g}_{np}=g_{np}$. This simplification concerning ϕ_x will not be applicable in calculations on atom–nonlinear triatomic molecule collisions,[52]

which will therefore prove considerably more expensive than the atom–linear triatomic case.

ϕ_x can now be omitted from the equations and p' and p'' are set to p. The close-coupling matrix elements can therefore be written

$$V^{v'',p}_{v',p}(R,\theta_x)=\int_{-\infty}^{\infty}\int_0^{\infty}\int_{-\infty}^{\infty}\int_0^{2\pi} dQ_1\,dQ_2\,dQ_3\,d\delta\,\psi_{v',p}(Q_1,Q_2,Q_3,\delta)$$
$$\times\psi_{v'',p}(Q_1,Q_2,Q_3,\delta)V_{\rm int}(R,\theta_x,Q_1,Q_2,Q_3,\delta)\,Q_2\ . \qquad (21)$$

The numerical techniques for evaluating these matrix elements, and solving the close-coupling equations are discussed in Sec. IID.

Application of the boundary conditions

$$f^{\bar{l}v\bar{p}}_{v'p}(R=0,\theta_x)=0$$

and

$$f^{\bar{l}v\bar{p}}_{v'p}(R,\theta_x)\xrightarrow[R\to\infty]{} k_{v'}^{-1/2}\{\delta_{vv'}\exp[-i(k_vR-\tfrac{1}{2}\bar{l}\pi)]$$
$$-S^{\bar{l}\bar{p}}_{v'v}(\theta_x)\exp[i(k_{v'}R-\tfrac{1}{2}\bar{l}\pi)]\} \qquad (22)$$

to the solution of Eq. (18) yields the angle-dependent S matrix elements $S^{\bar{l}\bar{p}}_{v'v}(\theta_x)$. In relating these to the exact S matrix elements the following analysis based on the method used in IOS studies of atom–diatom collisions,[14,15,18,41] is employed.

The total angular momentum eigenfunctions $\mathcal{Y}^{JM}_{j\bar{l}\bar{\lambda}}$ are constructed from[48]

$$\mathcal{Y}^{JM}_{j\bar{l}\bar{\lambda}}=\sum_{m_j}\sum_{m_l} C(lm_l jm_j JM)\bar{D}^{j}_{\bar{\lambda}m_j}Y^{m_l}_{l}\ , \qquad (23)$$

where

$$\bar{D}^{j}_{\bar{\lambda}m_j}=[(2j+1)/4\pi]^{1/2}D^{j}_{\bar{\lambda}m_j}\ . \qquad (24)$$

$Y^{m_l}_{l}$ are the spherical harmonics defined with respect to space-fixed axes. $C(lm_l jm_j JM)$ are the Clebsch–Gordan coefficients.[48]

If matrix elements over Eq. (18) are formed by multiplying on the left by $\mathcal{Y}^{JM}_{j'l'\bar{\lambda}'}$ and on the right by $\mathcal{Y}^{JM*}_{j\bar{l}\bar{\lambda}}$, we obtain

$$\left(\frac{d^2}{dR^2}+k^2_{v'}-\frac{\bar{l}(\bar{l}+1)}{R^2}\right)F^{J\bar{l}}_{\alpha'}(R)$$
$$=\left(\frac{2\mu}{\hbar^2}\right)\sum_{\alpha''}V^{J\alpha''}_{\alpha'}F^{J\alpha}_{\alpha''}(R)\ , \qquad (25)$$

where α represents the indices $(v,\bar{\lambda},j,p,l)$. Note that one of the four quantum numbers represented by v is λ. In constructing Eq. (25) the completeness of the $\mathcal{Y}^{JM}_{j\bar{l}\bar{\lambda}}$ has been used. The V and F functions in Eq. (25) are obtained by taking matrix elements over $V^{v'',p}_{v',p}$ and $f^{\bar{l}v\bar{p}}_{v'p'}$, respectively between the angular momentum functions. If we set $l'=\bar{l}$, $\bar{k}^2_{v',j'}=k^2_{v'}$, $\lambda=\bar{\lambda}$, $\lambda'=\bar{\lambda}'$, and $\lambda''=\bar{\lambda}''$, Eqs. (25) become the exact close-coupling equations for the Hamiltonian obtained by subtracting the $H^{V-R}_{\rm ABC}$ term from H. $H^{V-R}_{\rm ABC}$ couples together terms in λ and $\lambda\pm1$,[45] so that λ is not quite a good quantum number in the exact case. The $H^{V-R}_{\rm ABC}$ terms, however, are very small. For example for the low-lying levels of CO_2 the vibration–rotation terms in the second order perturbation expansion for the energy are two orders of magnitude smaller than the purely rotational terms.[40] Note that $\bar{k}^2_{v',j'}=(2\mu/\hbar^2)[E-\bar{E}_{v',j'}]$, where $\bar{E}_{v',j'}$ is the eigenvalue of $H^{V}_{\rm ABC}+H^{R}_{\rm ABC}$.

Forming the analogous matrix elements over the asymptotic solutions (22) of Eq. (18) yields the VCC–IOS approximation to the exact S matrix elements

$$S^{J\bar{p}}_{v'j'l'vjl}=i^{(l+l'-2\bar{l})}\int \mathcal{Y}^{JM}_{j'l'\lambda'}S^{\bar{l}\bar{p}}_{v'v}\mathcal{Y}^{JM*}_{jl\lambda}$$
$$\times\sin\theta\sin\theta'\,d\theta\,d\theta'\,d\phi\,d\phi'\ . \qquad (26)$$

The coordinate system is now rotated into the body-fixed (BF) frame in which the z axis is along **R**. In the BF frame θ', ϕ', and ϕ are all zero and θ goes over into θ_x. Substitution of[48]

$$\mathcal{Y}^{JM}_{j'l'\lambda'}=\sum_{N'}D^{J}_{N'M}(\bar{\chi},\bar{\theta},\bar{\phi})C(l'0j'N'JN')$$
$$\times\left(\frac{2l'+1}{4\pi}\right)^{1/2}\bar{D}^{j'}_{\lambda'N'}(\chi,\theta_x,0)\ , \qquad (27)$$

and the analogous formula for $\mathcal{Y}^{JM*}_{jl\lambda}$ into (26) yields an expression in which the integration over $\bar{\chi}$, $\bar{\theta}$, and $\bar{\phi}$ can at once be performed to give

$$S^{J\bar{p}}_{v'j'l'vjl}=\sum_{N}i^{(l+l'-2\bar{l})}C(l0jNJN)C(l'0j'NJN)$$
$$\times\frac{[(2l+1)(2l'+1)]^{1/2}2\pi}{2J+1}\int_0^{\pi}\bar{D}^{j'}_{\lambda'N}(\chi,\theta_x,0)$$
$$\times S^{\bar{l}\bar{p}}_{v'v}(\theta_x)\bar{D}^{j*}_{\lambda N}(\chi,\theta_x,0)\sin\theta_x\,d\theta_x\ . \qquad (28)$$

The exact state-to-state integral cross section for a transition from $(v,j)\to(v')$, summed over all j' states in level v', is given by[12]

$$\sigma^{p\bar{p}'}_{vjv'}=\frac{\pi}{k^2_{vj}}\sum_{J}^{\infty}\sum_{j'}\sum_{l'}\sum_{l}\frac{2J+1}{2j+1}$$
$$\times\left|\delta_{jvlp,j'v'l'p'}-S^{J\bar{p}'\bar{p}}_{v'j'l'vjl}\right|^2\ . \qquad (29)$$

where k_{vj} is the exact wavenumber for state (vj). In Eq. (29), k_{vj} is replaced by k_v and the exact S matrix element $S^{J\bar{p}'\bar{p}}_{v'j'l'vjl}$ is replaced by expression (28) for $S^{J\bar{p}}_{v'j'l'vjl}$, with $\bar{l}$ in Eq. (28) being set equal to l. The summations over l' and J can then be performed using the sum rule for Clebsch–Gordan coefficients,[49] while the sum over j' can be carried out using the completeness of the $\bar{D}^{j'}_{\lambda'N}$. The sum over N is then performed using the sum rule[42] for the $\bar{D}^{j}_{\lambda N}$. The resulting expression is independent of j. $\sigma^{p\bar{p}'}_{vjv'}$ is thus set to $\sigma^{\bar{p}}_{vv'}$ and we obtain

$$\sigma^{\bar{p}}_{vv'}=\frac{\pi}{2k^2_v}\int_0^{\pi}d\theta_x\sin\theta_x\sum_{l}(2l+1)\left|\delta_{vv'}-S^{l\bar{p}}_{v'v}(\theta_x)\right|^2\ . \qquad (30)$$

Solution of the close-coupling equations (18) over a grid of values of θ_x is therefore all that is required to yield the $\sigma^{\bar{p}}_{vv'}$ using this very simple formula. For a symmetric molecule, such as CO_2, it is only necessary to integrate Eq. (30) between 0 and $\frac{1}{2}\pi$, and the resulting expression is multiplied by 2.

The rate coefficient for a transition $v\to v'$ is[43]

$$k_{vv'}=\left(\frac{8k_BT}{\pi\mu}\right)^{1/2}\frac{1}{(k_BT)^2}Q^{-1}f_v\sum_j(2j+1)\exp\left(\frac{-E_{vj}}{k_BT}\right)$$
$$\times\sum_{\bar{p}}\sum_{\bar{p}'}\int_0^{\infty}E^{\rm tr}_{vj}\exp\left(\frac{-E^{\rm tr}_{vj}}{k_BT}\right)\sigma^{\bar{p}\bar{p}'}_{vjv'}(E^{\rm tr}_{vj})\,dE^{\rm tr}_{vj}\ . \qquad (31)$$

Note the distinction between $k_{vv'}$ and k_{vj}. In Eq. (31), k_B is the Boltzmann constant, T is temperature, Q is the rotational partition function, E_{vj} is the energy of the (v,j) state with respect to the $(v,j=0)$ state, and E_{vj}^{tr} is the translational energy of the (v,j) state. $\sigma_{vjv'}^{pp'}$ is defined in Eq. (29). f_v is a degeneracy factor which accounts for the degeneracy of the $p=o$ and $p=e$ levels for $\lambda>0$ and has the values

$$f_v=1 \text{ for } \lambda=0\,, \quad f_v=\tfrac{1}{2} \text{ for } \lambda>0\,. \tag{32}$$

In the VCC–IOS approximation $E_{vj}=0$, and $E_{vj}^{tr}=E_v^{tr}=E-E_v$. After replacing $\sigma_{vjv'}^{pp'}$ by $\sigma_{vv'}^{p}$, expression (31) becomes

$$k_{vv'}=\left(\frac{8k_BT}{\pi\mu}\right)^{1/2}\frac{1}{(k_BT)^2}f_v\sum_p\int_0^\infty E_v^{tr}\times\exp\left(\frac{-E_v^{tr}}{k_BT}\right)\sigma_{vv'}^{p}(E_v^{tr})\,dE_v^{tr}\,. \tag{33}$$

C. Potentials for X-CO_2

The CO_2 potential used in all the calculations was of the realistic anharmonic form

$$V_{CO_2}=V_m(\Delta R_1)+V_m(\Delta R_2)+F_R\,\Delta R_1\Delta R_2+\tfrac{1}{2}F_\alpha R_e^2\Delta\alpha^2\,, \tag{34}$$

where

$$V_m(\Delta R)=D_e[1-\exp(-\alpha_M\Delta R)]^2\,. \tag{35}$$

ΔR_1 and ΔR_2 are the displacements of the CO bond lengths from equilibrium, and $\Delta\alpha$ is the deviation of the O–C–O bond angle from 180°. The constants in V_{CO_2} were $D_e=5.453$ eV, $\alpha_M=1.6024a_0^{-1}$, $R_e=2.1948a_0$, $F_R=2.2166$ eV a_0^{-2}, and $F_\alpha=1.0174$ eV a_0^{-2}. These constants were obtained from analysis of spectroscopic data.[50]

Substitution of V_{CO_2} and H_{cor} into H_{ABC}^V [Eq. (2)] yields the vibrational CO_2 Hamiltonian H_{CO_2} which is diagonalized using the basis set defined in Eq. (10). The matrix elements in the secular equations were computed using numerical methods described in Sec. IID. V_{CO_2} is expressed in terms of normal coordinates by first express ing ΔR_1, ΔR_2, and $\Delta\alpha$ in terms of Cartesians and then using Eq. (8).

The atom–CO_2 interaction potentials were of the pairwise form used by Suzukawa *et al.*[28]

$$V_{int}=\sum_{i=1}^{3}V_x(R_i)\,. \tag{36}$$

TABLE I. Potential parameters in V_{int} and V_x.

X	R_0 (a_0)[a]	ϵ_0 (eV)[b]	B (a_0^{-1})[c]
He	5.9	3.5×10^{-3}	2.06
Ne	5.7	1.1×10^{-2}	2.12
Ar	6.3	1.8×10^{-2}	2.72

[a]X–C distance at minimum of V_{int}.
[b]Well depth at minimum of V_{int}.
[c]Exponent B of exponential short range part of ESMSV function $V_x(R_i)$.

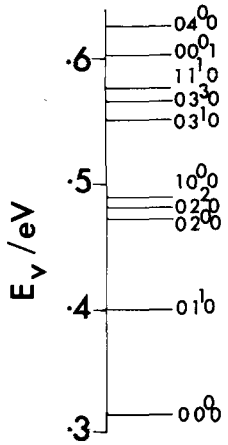

FIG. 2. Energy levels of CO_2 $(v_1v_2^\lambda v_3)$ plotted against E_v.

The pair potentials $V_x(R_i)$ were taken to be of the ESMSV form[36,37] in which an exponential function is connected by an exponential spline function to a Morse function which is connected by another spline function to a van der Waals function. The parameters used in the ESMSV functions for He, Ne, and Ar were those derived for the systems He–Ne, Ne–Ne, and Ar–Ne, respectively, from molecular beam and virial coefficient data.[36,37] The ESMSV parameters for Ne and Ar were taken from Table II, Ref. 28, while the parameters for He were taken from Table II, Ref. 36.

In Table I the exponents of the short range exponential parts of $V_x(R_i)$ are tabulated for He, Ne, and Ar. Also tabulated are the X–C distance (R_0) and well depth (ϵ_0) at the minimum in V_{int}. All X–CO_2 systems are T shaped at the minimum position, with the well depth increasing with increasing mass. The R_0 and ϵ_0 values for He–CO_2 ($5.9a_0$ and 3.5×10^{-3} eV) agree well with the values ($6.25a_0$ and 3.9×10^{-3} eV) determined recently from differential cross section experiments.[17]

D. Numerical techniques

To evaluate the matrix elements of the secular equations for the basis set (10) and Hamiltonian H_{CO_2}, Gauss–Hermite quadrature was used for the integration over Q_1 and Q_3, while Gauss–Laguerre quadrature was used for the integration over Q_2.[44,45] These schemes integrate exactly integrals of the form

$$\int_a^\infty\sum_{j=1}^{N+1}C_jQ^{j-1}\exp(-tQ^n)\,dQ\,, \tag{37}$$

provided $N\leq2M-1$, where M is the number of integration points. For $Q=Q_1$ or Q_3, $a=-\infty$ and $n=2$, while for $Q=Q_2$, $a=0$ and $n=1$. The integration over δ is performed analytically when diagonalizing H_{CO_2}.

In Fig. 2 the first ten energy levels of CO_2, obtained using a total of 61 basis functions, are displayed. The usual harmonic-oscillator notation $(N_1N_2^\lambda N_3)$ is used to label these anharmonic levels, although it is important to note that several levels which are close in energy and have the same value for λ are in strong Fermi resonance. For example, the wave functions for the third and fifth levels ϕ_3 and ϕ_5 [which we denote (02^00) and (10^00), respectively] are

$$\phi_3 = 0.65\,|10^00\rangle - 0.76\,|02^00\rangle$$
and
$$\phi_5 = 0.76\,|10^00\rangle + 0.65\,|02^00\rangle\ . \tag{38}$$

In Eqs. (38) only the leading terms are included and $|m_1 m_2^{\lambda} m_3\rangle$ is a normalized harmonic basis function. Other levels in Fermi resonance are (03^10) and (11^10).

The close-coupling matrix elements $V_{v'\rho}^{v''\rho}(R,\theta_x)$ defined in Eq. (21) are computed with the same Gauss–Hermite and Gauss–Laguerre integration points and weights that were used in diagonalizing H_{CO_2}, with the addition of an equal spacing quadrature for the integration over δ. In computing $V_{v'\rho}^{v''\rho}$ considerable computer time was saved by initially storing the pre-exponential part of the normalized molecular eigenfunctions $\{\psi_{v\rho}^{e}(Q_1,Q_2,Q_3,\delta)\}$ at every quadrature point needed. The $V_{v'\rho}^{v''\rho}$ were then computed from

$$V_{v'\rho}^{v''\rho}(R,\theta_x) = \sum_{i_1}^{N_1}\sum_{i_2}^{N_2}\sum_{i_3}^{N_3}\sum_{i_4}^{N_4} w_1(i_1)w_2(i_2)w_3(i_3)w_4(i_4) \times \psi_{v''\rho}^{e}(Q_{1i_1},Q_{2i_2},Q_{3i_3},\delta_{i_4})\psi_{v'\rho}^{e}(Q_{1i_1},Q_{2i_2},Q_{3i_3},\delta_{i_4}) \times V_{int}(R,\theta_x,Q_{1i_1},Q_{2i_2},Q_{3i_3},\delta_{i_4})\ . \tag{39}$$

$w_j(i_j)$ is the weight for quadrature point i_j. The R_i in the original expression for V_{int} are related to the normal coordinates using Eqs. (15) and (8).

The close-coupling equations (18) were solved using the R matrix propagation method.[46] In this approach the X–CO_2 distance R is divided up into small sectors with midpoints $R=R_m$. It is necessary to diagonalize the matrices $\mathbf{A}^{\rho}$ with elements

$$\mathbf{A}^{\rho}_{v''v'} = E_{v'}\,\delta_{v'v''} + V_{v'\rho}^{v''\rho}(R_m,\theta_x) \tag{40}$$

for all chosen values of R_m. The eigensolutions obtained in this way are evaluated and stored once and used for calculations at all energies and all required values of l. It is necessary to perform these diagonalizations for all chosen values of θ_x.

In diagonalizing $\mathbf{A}^{\rho}$, the first N molecular eigenfunctions $\{\psi_{v\rho}\}$ were used as a basis set. For the actual propagation of the R matrix from sector to sector,[46] the first M_1+M_2 eigenfunctions obtained in the diagonalization of $\mathbf{A}^{\rho}$ were used, where M_1 is the number of asymptotically open channels and M_2 is a chosen number of asymptotically closed channels ($M_1+M_2 \le N$). S matrix elements were obtained over a grid of values of θ_x at points corresponding to a Simpson's rule quadrature. The $\sigma_{vv'}^{\rho}$ were then obtained directly by using Simpson's rule for evaluating Eq. (30).

The accuracy of the numerical techniques described above was checked by examining the effect on $\sigma_{vv'}^{\rho}$ of reducing the numerical integration step lengths or increasing the number of basis functions used. To obtain $\sigma_{vv'}^{\rho}$ for He and Ne converged to within 1% for total energies E_{tot} between 0.40 and 0.68 eV, and for Ar converged to within 3% for total energies E_{tot} between 0.40 and 0.60 eV, the following numerical procedures were required. Sixty-one basis functions [defined in Eq. (10)] were needed to diagonalize H_{CO_2} with Q_1, Q_2, and Q_3 having maximum powers of 4, 6, and 4, respectively. The number of quadrature points needed in computing $V_{v'\rho}^{v''\rho}$ was 8, 12, 8, and 10 for the integration over Q_1, Q_2, Q_3, and δ, respectively. For He, Ne, and Ar, 40, 55, and 120 R matrix sectors were required. A maximum of 14 molecular eigenfunctions were needed in diagonalizing $\mathbf{A}^{\rho}$ [Eq. (40)], while up to two asymptotically closed channels were required in propagating R matrix solutions from sector to sector. The number of quadrature points over θ_x needed to compute Eq. (30) were 7, 9, and 11 for He, Ne, and Ar, respectively. The maximum values of l required were 63, 89, and 112 for He, Ne, and Ar, respectively.

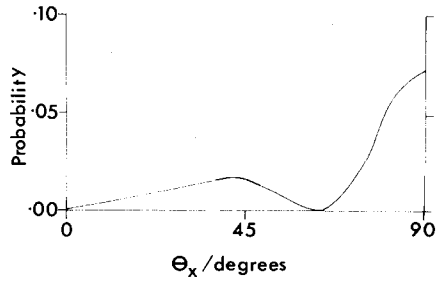

FIG. 3. θ_x dependence of the probability $|S^{l=0,\rho=e}_{(00^00)(01^10)}|^2$ for X = He and $E_{tot} = 0.5$ eV.

The rate coefficients $k_{vv'}$ [Eq. (33)] were computed by fitting a cubic spline function to the $\sigma_{vv'}^{\rho}$ and then using Simpson's rule. We needed 20 min of CDC 7600 computer time to compute converged cross sections at ten energies between $E_{tot}=0.40$ eV and $E_{tot}=0.68$ eV for He. This was sufficient to give converged rate coefficients for transitions involving the first five levels of CO_2 for temperatures up to 300 K. About one-fifth of this time was needed to construct the necessary $V_{v'\rho}^{v''\rho}$.

The computer program developed using the procedures described above is automatic and general and should be applicable to many other atom–vibrating linear triatomic molecule collisions with potentials in any realistic numerical or functional form. Furthermore, it is straightforward to adapt the methods and computer program described here to enable atom–vibrating nonlinear triatomic molecule collisions to be studied.[52]

III. CALCULATIONS

Calculations of $\sigma_{vv'}^{\rho}$, with $p=e$ and o, were performed over a grid of energies between $E_{tot}=0.40$ and 0.68 eV for X = He and Ne and between $E_{tot}=0.40$ and 0.60 eV for X = Ar.

A. Angle dependence

In Fig. 3 the θ_x dependence of the He transition probability $|S_{vv'}^{l=0,\rho=e}(\theta_x)|^2$ is plotted for $v=(00^00)$, $v'=(01^10)$, and $E_{tot}=0.5$ eV. This demonstrates the strong dependence on θ_x of these quantities. In a quasiclassical study[28] on Ne, Ar, and Kr collisions with CO_2, similar angular dependencies were observed. VCC–IOS calculations on atom–diatom collisions also illustrate strong angular dependencies of this kind.[18] It can be seen from Eqs. (8) and (15) that for $\theta_x=0°$, V_{int} is independent of Q_2 and thus S matrix elements for transitions such as

TABLE II. $\sigma_{vv'}^{p=e}/a_0^2$ for X = He, Ne, and Ar. $E_{tot} = 0.60$ eV. Entries in each vertical block are for He, Ne, and Ar, respectively. Numbers in parentheses denote powers of 10 by which entries should be multiplied.

$v \backslash v'$	(00^00)	(01^10)	(02^00)	(02^20)	(10^00)	(03^10)	(03^30)	(11^10)
(00^00)		0.11(+1)	0.47(−2)	0.58(−2)	0.21(−2)	0.18(−4)	0.34(−5)	0.68(−6)
		0.20	0.21(−3)	0.95(−4)	0.20(−4)	0.46(−6)	0.21(−6)	0.22(−6)
		0.19	0.39(−2)	0.63(−3)	0.77(−3)	0.96(−5)	0.42(−5)	0.17(−5)
(01^10)	0.16(+1)		0.29	0.38	0.13	0.15(−2)	0.28(−3)	0.79(−4)
	0.29		0.60(−1)	0.31(−1)	0.54(−2)	0.28(−4)	0.32(−5)	0.19(−5)
	0.27		0.43(−1)	0.85(−1)	0.35(−1)	0.96(−3)	0.59(−4)	0.94(−4)
(02^00)	0.11(−1)	0.46		0.16	0.18	0.10	0.36(−3)	0.17(−3)
	0.47(−3)	0.95(−1)		0.61	0.61	0.29(−2)	0.29(−4)	0.48(−5)
	0.86(−2)	0.68(−1)		0.67	0.61	0.38(−1)	0.69(−3)	0.21(−3)
(02^20)	0.14(−1)	0.65	0.17		0.21	0.30(−1)	0.50(−1)	0.14(−2)
	0.23(−3)	0.54(−1)	0.67		0.97	0.24(−2)	0.75(−3)	0.37(−4)
	0.15(−2)	0.15	0.72		0.12(+1)	0.53(−2)	0.30(−1)	0.13(−2)
(10^00)	0.55(−2)	0.23	0.21	0.23		0.14(−1)	0.36(−3)	0.16(−1)
	0.53(−4)	0.99(−2)	0.71	0.10(+1)		0.21(−2)	0.49(−4)	0.16(−3)
	0.20(−2)	0.65(−1)	0.71	0.13(+1)		0.25(−2)	0.16(−2)	0.11(−1)
(03^10)	0.11(−3)	0.64(−2)	0.28	0.77(−1)	0.34(−1)		0.57(−1)	0.44(−1)
	0.29(−5)	0.12(−3)	0.81(−2)	0.60(−2)	0.49(−2)		0.19	0.54(−1)
	0.59(−4)	0.42(−2)	0.10	0.14(−1)	0.59(−2)		0.40	0.82(−1)
(03^30)	0.29(−4)	0.17(−2)	0.14(−2)	0.17	0.12(−2)	0.79(−1)		0.42(−1)
	0.18(−5)	0.19(−4)	0.11(−3)	0.26(−2)	0.16(−3)	0.26		0.15
	0.36(−4)	0.36(−3)	0.26(−2)	0.11	0.52(−2)	0.56		0.38
(11^10)	0.89(−5)	0.74(−3)	0.99(−3)	0.74(−2)	0.79(−1)	0.93(−1)	0.65(−1)	
	0.29(−5)	0.18(−4)	0.28(−4)	0.20(−3)	0.83(−3)	0.11	0.24	
	0.22(−4)	0.87(−3)	0.12(−2)	0.73(−2)	0.57(−1)	0.18	0.59	

$(00^00) \rightarrow (01^10)$ at $\theta_x = 0°$ are zero. At $\theta_x = 90°$, V_{int} is independent of Q_1 and Q_3 and thus, if a harmonic CO_2 potential is used, S matrix elements for transitions such as $(00^00) \rightarrow (00^01)$ or $(00^00) \rightarrow (10^00)$ are zero for $\theta_x = 90°$.

B. Cross sections involving bending and symmetric stretch modes

In Table II the cross sections $\sigma_{vv'}^{p=e}$ are tabulated for X = He, Ne, and Ar with $E_{tot} = 0.60$ eV. The analogous results for $\sigma_{vv'}^{p=o}$ are presented in Table III. At this energy the first eight vibrational levels are open.

These calculations show that the magnitude of the energy difference $\Delta E_{vv'}$ between two levels v and v' largely determines $\sigma_{vv'}^{p}$. The smaller the value of $\Delta E_{vv'}$, the larger the magnitude of $\sigma_{vv'}^{p}$. Thus, for example, for transitions from the ground state $v = (00^00)$, $\sigma_{vv'}^{p}$ for $v' = (01^10)$ is two orders of magnitude larger than the $\sigma_{vv'}^{p}$ for which $v' = (02^00)$, (02^20), or (10^00). And these latter three cross sections are themselves two orders of magnitude larger than those for which $v' = (03^10)$, (03^30), or (11^10). When $\Delta E_{vv'}$ and $\Delta E_{vv''}$ are similar, transitions into the level which has the lowest energy are favored. For example for $v = (01^10)$, transitions into $v' = (00^00)$ have larger $\sigma_{vv'}^{p}$ than the transition with $v' = (02^00)$.

Overall, there are no exceptionally pronounced selection rules for transitions with particular values of the vibrational angular momentum quantum number λ. For example, the transition with $v = (00^00)$ and $v' = (02^20)$ has a cross section comparable in magnitude to those for which $v' = (02^00)$ or $v' = (10^00)$. When comparing $\sigma_{vv'}^{p}$ for the two groups with $p = e$ and $p = o$ it is striking that many values with the same v and v' are similar, particularly for large λ or λ'. For example, the $\sigma_{vv'}^{p}$ for $v = (02^20)$ and $v' = (03^30)$ for the He collision is $0.050 a_0^2$ with $p = e$ and $0.052 a_0^2$ for $p = o$.

Near resonant transitions have quite large cross sections, which increase with increasing mass of atom X. For example, $\sigma_{vv'}^{p}$ for the transitions $(02^20) \rightarrow (02^00)$ and $(03^30) \rightarrow (11^10)$ are largest for Ar and smallest for He. $\sigma_{vv'}^{p}$ for transitions between levels with larger $\Delta E_{vv'}$ [for

TABLE III. Same as for Table II, except for $\sigma_{vv'}^{p=o}$.

$v \backslash v'$	(01^10)	(02^20)	(03^10)	(03^30)	(11^10)
(01^10)		0.40	0.20(−3)	0.31(−3)	0.11(−4)
		0.31(−1)	0.13(−4)	0.58(−5)	0.15(−5)
		0.11	0.99(−3)	0.53(−4)	0.65(−4)
(02^20)	0.68		0.32(−1)	0.52(−1)	0.14(−2)
	0.54(−1)		0.27(−2)	0.82(−3)	0.29(−4)
	0.19		0.82(−2)	0.22(−1)	0.12(−2)
(03^10)	0.87(−3)	0.82(−1)		0.48(−1)	0.19(−1)
	0.57(−4)	0.67(−2)		0.17	0.21(−1)
	0.43(−2)	0.21(−1)		0.28	0.28(−1)
(03^30)	0.18(−2)	0.18	0.66(−1)		0.37(−1)
	0.35(−4)	0.29(−2)	0.24		0.16
	0.32(−3)	0.77(−1)	0.38		0.52
(11^10)	0.11(−3)	0.75(−2)	0.41(−1)	0.58(−1)	
	0.14(−4)	0.16(−3)	0.46(−1)	0.25	
	0.61(−3)	0.66(−2)	0.60(−1)	0.81	

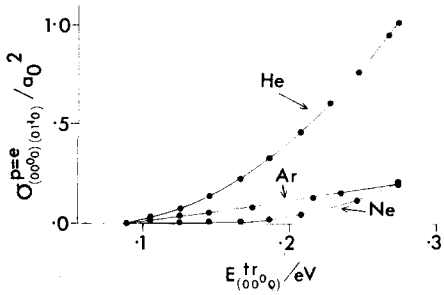

FIG. 4. $\sigma^{p=e}_{(00^00)(01^10)}$ plotted as a function of $E^{tr}_{(00^00)}$ for X = He, Ne, and Ar.

example, for $(00^00) \rightarrow (01^10)$] are largest for He.

In Fig. 4, the $\sigma^{p}_{vv'}$ for X = He, Ne, and Ar with $v = (00^00)$ and $v' = (01^10)$ are plotted as functions of the translational energy E^{tr}_{v} defined with respect to the $v = (00^00)$ state. It can be seen that the $\sigma^{p}_{vv'}$ for He are largest and rise much more steeply with E^{tr}_{v} than those for Ne or Ar. The $\sigma^{p}_{vv'}$ for Ar is larger than that for Ne except at the highest energy. The $\sigma^{p}_{vv'}$ for Ne rise more steeply with E^{tr}_{v} than those for Ar. In Fig. 5 similar plots for He and Ne are made of the $\sigma^{p}_{vv'}$ with $v = (02^00)$ and $v' = (01^10)$ or $v' = (02^20)$. For He, the cross section with $v' = (01^10)$ is larger than that for which $v' = (02^20)$ over the whole energy range. The reverse is true for Ne however, the transition with $v' = (02^20)$ being favored. These results emphasize the observation made before: increasing the mass of X increases $\sigma^{p}_{vv'}$ for near resonant transitions.

It can be seen from the results of Tables II and III and Fig. 4 that in almost every case the $\sigma^{p}_{vv'}$ for Ar are greater than those for Ne. To determine whether this is due to a mass or a potential energy surface effect, calculations for He, Ne, and Ar were all performed with the same interaction potential

$$V^{ex}_{int} = \sum_{i=1}^{3} 330.6 \exp(-2.06 R_i) \ . \qquad (41)$$

V^{ex}_{int} is in units of eV and R_i is in a_0. The parameters in Eq. (41) are those of the exponential part of the ESMSV potential for He.[36] In Table IV calculations of

TABLE IV. $\sigma^{p=e}_{vv'}/a_0^2$ as for Table II, except using ESMSV and exponential potentials V^{ex}_{int} [Eq. (41)]. $E_{tot} = 0.56$ eV.

	Interaction potentials	
Transition	ESMSV	V^{ex}_{int}
$(00^00) \rightarrow (01^10)$	0.77	0.14
	0.11	0.19(−2)
	0.17	0.15(−3)
$(02^00) \rightarrow (01^10)$	0.29	0.28(−1)
	0.39(−1)	0.19(−3)
	0.52(−1)	0.10(−4)
$(02^00) \rightarrow (02^20)$	0.12	0.40(−1)
	0.44	0.86(−1)
	0.56	0.92(−1)

TABLE V. $\sigma^{p=e}_{vv'}/a_0^2$ for X = He and Ne. $v = (00^01)$ and $E_{tot} = 0.64$ eV. Numbers in parentheses denote powers of 10 by which entries should be multiplied.

v'	He	Ne
(00^00)	0.70(−6)	0.56(−4)
(01^10)	0.16(−5)	0.16(−5)
(02^00)	0.18(−4)	0.33(−5)
(02^20)	0.78(−6)	0.15(−6)
(10^00)	0.53(−4)	0.14(−5)
(03^10)	0.34(−4)	0.20(−4)
(03^30)	0.35(−6)	0.81(−6)
(11^10)	0.11(−3)	0.20(−3)
(04^00)	0.18(−4)	0.19(−4)

$\sigma^{p}_{vv'}$ obtained using V^{ex}_{int} are reported for He, Ne, and Ar for the transitions $(00^00) \rightarrow (01^10)$, $(02^00) \rightarrow (02^20)$, and (01^10), respectively. The total energy is $E_{tot} = 0.56$ eV. These results are compared with those obtained using the ESMSV forms for V_{int}, which are different for each atom X. It can be seen that for the transition $(00^00) \rightarrow (01^10)$, the $\sigma^{p}_{vv'}$ are smaller for Ar than for Ne with the V^{ex}_{int} potential while the reverse is true with the ESMSV potentials. Therefore the fact that $\sigma^{p}_{vv'}$ for $(00^00) \rightarrow (01^10)$ is larger for Ar than Ne over most of the energy range of Fig. 4 is due to the differences in the ESMSV potential energy surfaces. In particular, the Ar ESMSV potential has a deeper well and is more repulsive at short range than the Ne ESMSV potential. For the transitions with $v = (02^00)$ and $v' = (02^20)$, $\sigma^{p}_{vv'}$ follow the relationship Ar > Ne > He on both types of potential energy surface. Note also that all the $\sigma^{p}_{vv'}$ for the potential V^{ex}_{int} are smaller than those for the ESMSV potentials, thus implying that the ESMSV potentials are more efficient at inducing vibrational excitation at these energies.

C. Deactivation of the asymmetric stretch mode

Some limited calculations were performed with X = He and Ne at energies such that deactivation of the first excited asymmetric stretch level (00^01) could be studied. In Table V, $\sigma^{p}_{vv'}$ for $v = (00^01)$ are presented with $E_{tot} = 0.64$ eV. For both the He and Ne cases the $\sigma^{p}_{vv'}$ for $v' = (11^10)$ is largest. First order perturbation calculations[3,5,34] on Ne + CO_2 (00^01) also predict that the transition with $v' = (11^10)$ is favored. For He we find that the next largest $\sigma^{p}_{vv'}$ are for $v' = (03^10)$ and $v' = (10^00)$. For

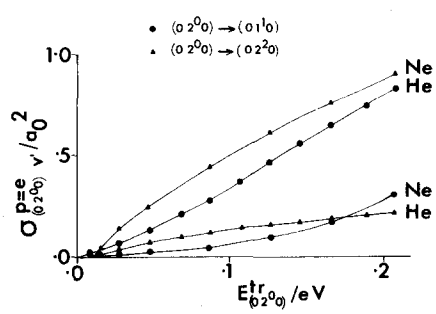

FIG. 5. $\sigma^{p=e}_{(02^00)v'}$ plotted as a function of $E^{tr}_{(02^00)}$ for X = He and Ne. $v' = (01^10)$ (circles) or $v' = (02^20)$ (triangles).

TABLE VI. $k_{vv'}$/molecule^{-1} cm^3 sec^{-1} for X = He, Ne, and Ar at $T = 300$ K. Entries in each vertical block are for He, Ne, and Ar, respectively. Numbers in parentheses denote powers of 10 by which entries should be multiplied.

$v \backslash v'$	(00^00)	(01^10)	(02^00)	(02^20)	(10^00)
(00^00)		0.39(−13) 0.14(−14) 0.66(−14)	0.23(−16) 0.14(−17)	0.12(−16) 0.52(−18)	0.76(−17) 0.50(−18)
(01^10)	0.49(−12) 0.17(−13) 0.85(−13)		0.17(−13) 0.12(−14)	0.32(−13) 0.11(−14)	0.46(−14) 0.11(−15)
(02^00)	0.10(−13) 0.62(−15)	0.60(−12) 0.42(−13)		0.24(−12) 0.48(−12)	0.21(−12) 0.30(−12)
(02^20)	0.77(−14) 0.13(−15)	0.86(−12) 0.28(−13)	0.18(−12) 0.35(−12)		0.19(−12) 0.45(−12)
(10^00)	0.69(−14) 0.43(−15)	0.32(−12) 0.66(−14)	0.43(−12) 0.59(−12)	0.51(−12) 0.12(−11)	

Ne the second largest $\sigma^{\flat}_{vv'}$ has $v' = (00^00)$. Transitions into levels with large λ', such as (03^30) and (02^20), have notably small $\sigma^{\flat}_{vv'}$.

The degeneracy averaged deactivation cross section is defined by

$$\sigma_v^D = \sum_{v'} \sum_{\flat} f_v \sigma^{\flat}_{vv'} , \tag{42}$$

where f_v is defined in Eq. (32).

For $v = (00^01)$ and $E_{tot} = 0.64$ eV ($E_v^{tr} = 0.035$ eV), $\sigma_v^D = 0.00024 a_0^2$ for He and $0.00030 a_0^2$ for Ne. These values are smaller than those obtained for the σ_v^D of the lower levels such as (01^10) at similar values of E_v^{tr}. For example, with $v = (01^10)$ and $E_v^{tr} = 0.022$ eV, $\sigma_v^D = 0.039 a_0^2$ for He and $0.0022 a_0^2$ for Ne. Note that σ_v^D is larger for He than Ne for $v = (01^10)$, while the reverse is true for $v = (00^01)$ at these values of E_v^{tr}. These limited calculations therefore support the experimental observations[3,5,6] that increasing the mass of X increases the ratio of the σ_v^D of the (00^01) state to the σ_v^D of lower states such as (01^10). Unfortunately, calculations were not performed over a large enough energy range to provide rate coefficients for deactivation of the (00^01) level for detailed comparison with experiments.

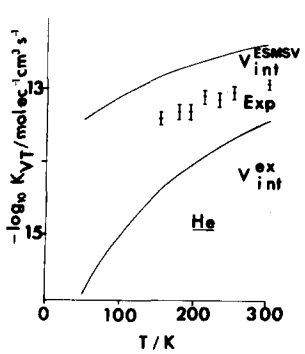

FIG. 6. $-\log_{10} K_{VT}$ plotted against T for X = He. (ǂ) Experiment (Ref. 3); (—) calculations using ESMSV form for V_{int} (V_{int}^{ESMSV}) or exponential form for V_{int} (V_{int}^{ex}).

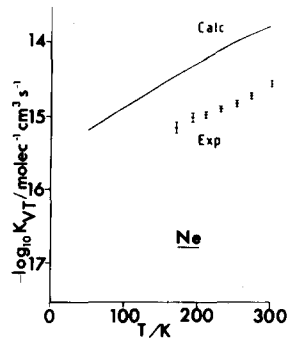

FIG. 7. $-\log_{10} K_{VT}$ plotted against T for X = Ne. (ǂ) Experiment (Ref. 3); (—) calculations using ESMSV potential.

D. Rate coefficients

Calculations of the rate coefficients $k_{vv'}$ defined in Eq. (33) were made for transitions involving the first five vibrational levels for X = He and Ne and for transitions involving the first two vibrational levels for X = Ar. The results for the temperature of 300 K are presented in Table VI. The $k_{vv'}$ follow the same patterns as those discussed in Sec. III B for the $\sigma^{\flat}_{vv'}$. They depend largely on $\Delta E_{vv'}$; for $v = (00^00)$ the $k_{vv'}$ with $v' = (01^10)$ is much larger than those for higher v' levels. Near resonant transitions such as $(02^00) \rightarrow (02^20)$ have larger $k_{vv'}$ for Ne than for He, while the reverse is true for transitions with larger $\Delta E_{vv'}$ which follow the relationship He > Ar > Ne.

Many of the $k_{vv'}$ presented in Table VI have not been measured or computed before. $k_{vv'}$ for the deactivation of (01^10) have been measured, however, and these are discussed in the next section.

E. Deactivation of the bending mode: Comparison with experiment

Studies of vibrational–translational energy transfer rate coefficients for the processes

$$CO_2(v_1 v_2^{\lambda} 0) + X \rightarrow CO_2(v_1' v_2'^{\lambda'} 0) + X \tag{II}$$

have been made in a variety of experiments.[1–3,7] Recent photoacoustic experiments[3] with X = He, Ne, Ar, Kr, and Xe have been made on the rate coefficients K_{VT} where

$$K_{VT} = k_{(01^10)(00^00)} + \Delta K \tag{43}$$

and

$$\Delta K = \sum_{v''}^{3} 2 \exp\left(\frac{-\Delta E_{v'',v}}{k_B T}\right)(k_{v'',v} - k_{vv'}) , \tag{44}$$

$$v = (01^10), \quad v' = (00^00), \quad v'' = (02^00), (02^20), (10^00) .$$

For temperatures below 300 K, ΔK is less than 10% of K_{VT}. For example in our calculations with X = He, $K_{VT} = 0.45 \times 10^{-12}$ molecule^{-1} cm^3 sec^{-1} while $\Delta K = -0.44 \times 10^{-13}$ molecule^{-1} cm^3 sec^{-1} at $T = 300$ K. Thus, to a good approximation, $K_{VT} = k_{(01^10)(00^00)}$ at the temperatures considered here.

In Figs. 6, 7, and 8 the calculated K_{VT} [obtained using

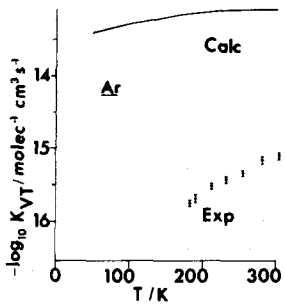

FIG. 8. As for Fig. 7 except X = Ar.

Eq. (43)] are compared with the experimental results for X = He, Ne, and Ar, respectively. Results for temperatures up to 300 K are displayed. For He and Ne the calculated K_{VT} are too large by a factor of 5, although the temperature dependence of the theoretical K_{VT} compares well with experiment. In Fig. 6 the K_{VT} for X = He, obtained in calculations using the exponential potential $V_{\text{int}}^{\text{ex}}$ defined in Eq. (41) are also presented. These are smaller than the experimental values and decrease too rapidly with decreasing temperature. This suggests that the ESMSV potential is of a more realistic form than $V_{\text{int}}^{\text{ex}}$.

For X = Ar, the calculated K_{VT} are much larger than the experimental results. The comparison of the theoretical and experimental temperature dependence of the K_{VT} for X = Ar is not so satisfactory as for X = He and Ne, the calculated K_{VT} having a temperature dependence that is too shallow for X = Ar.

Considering the fact that the atom–CO_2 interaction potentials used here are so approximate, the comparison between theory and experiment is quite encouraging. The errors in the calculated rate coefficients for He and Ne are of the same order of magnitude as the errors found typically in quantum calculations of vibrational deactivation rate coefficients for atom–diatom systems such as[47] $He + H_2(v = 1) \rightarrow He + H_2(v = 0)$.

IV. CONCLUSION

A combined vibrational close-coupling and rotational infinite order sudden method has been described for calculating vibrational excitation cross sections for atom–linear triatomic molecule collisions in three dimensions. The method has been successfully applied to the collisions of $X + CO_2$, where X = He, Ne, and Ar, over an energy range sufficient to provide rate coefficients for transitions involving the lower CO_2 vibrational levels for temperatures up to 300 K. From a study of both cross section and rate coefficient data, the following conclusions were obtained.

Propensities for particular vibrational transitions are determined largely by the energy difference $\Delta E_{vv'}$ between energy levels. For example, excitation of the ground state $(0\,0^0\,0)$ to the state nearest in energy, the first excited bending state (01^10), is favored. For calculations on the same potential energy surface, cross sections for transitions with relatively large $\Delta E_{vv'}$ decrease with increasing mass of X, while cross sections for near resonant transitions such as $(02^20) \rightarrow (02^00)$ increase with the mass of X. For calculations on the ESMSV potentials used in the majority of the present calculations which are different for each atom X, it is found that cross sections for Ar collisions are almost always larger than cross sections for Ne collisions.

It is found that deactivation of the first excited asymmetric stretch level (00^01) to the (11^10) level is favored over other transitions in agreement with previous first-order perturbation calculations.[3,5,34] The deactivation cross section for the (00^01) level at a given translational energy is smaller than those for the lower levels such as (01^10), although it does become larger, relative to the lower levels, as the mass of atom X is increased. This is in agreement with experimental findings.[3,5,6]

Comparison of calculated and experimental[3] rate coefficients for the deactivation of the CO_2 bending mode level, (01^10), is quite encouraging considering the approximate nature of the potentials used. Calculated results of these rate coefficients for X = He and Ne were within a factor of 5 of the experimental results and had the correct temperature dependence. The calculations for X = Ar were much larger than the experimental results and the calculated temperature dependence was not steep enough in this case.

In performing dynamical calculations on atom–vibrating linear triatomic molecule collisions it is necessary at the present time to resort to the use of very approximate atom–molecule interaction potential energy surfaces, as has been done here and in previous calculations.[21–33] Nevertheless, the results presented in this work show that calculations using approximate potentials do have some value in determining whether propensities for particular types of vibrational transitions exist. However, in making comparisons with experiment, it has been difficult to establish with certainty whether differences are due to the approximations inherent in the theory or the potential energy surface. Now that a realistic 3D quantum-dynamical method and computer program has been developed for yielding quantities such as vibrational deactivation rate coefficients for atom–linear triatomic molecule collisions, it will be worthwhile to invest in the expense of using accurate *ab initio* methods of calculation to yield realistic potentials, with full vibrational dependence, for systems such as $He–CO_2$.

ACKNOWLEDGMENTS

Support of this research by the Science Research Council is gratefully acknowledged. The numerical calculations were carried out on the CDC 7600 computer of the University of Manchester Regional Computer Centre.

[1] T. L. Cottrell and M. A. Day, *Molecular Relaxation Processes* (Academic, New York, 1966), p. 253.
[2] C. J. S. M. Simpson and T. R. D. Chandler, Proc. R. Soc. London Ser. A 317, 265 (1970).
[3] F. Lepoutre, G. Louis, and J. Taine, J. Chem. Phys. 70, 2225 (1979).

[4]W. Eastes, U. Ross, and J. P. Toennies, J. Chem. Phys. 66, 1919 (1977).
[5]J. T. Yardley and C. B. Moore, J. Chem. Phys. 46, 4491 (1967).
[6]C. B. Moore, R. E. Wood, B. Hu, and J. T. Yardley, J. Chem. Phys. 46, 4222 (1967).
[7]D. C. Allen, T. J. Price, and C. J. S. M. Simpson, Chem. Phys. Lett. 45, 183 (1977).
[8]P. K. Cheo, *Lasers*, Vol. 3, edited by A. K. Levine and A. J. DeMaria (Dekker, New York, 1971), p. 111.
[9]W. W. Duley, *CO_2 Lasers: Effects and Applications* (Academic, New York, 1976).
[10]R. M. Osgood Jr., Appl. Phys. Lett. 28, 342 (1976).
[11]K. Smith and R. M. Thomson, *Computer Modeling of Gas Lasers* (Plenum, New York, 1978), Chap. 2.
[12]A. S. Dickinson, Comput. Phys. Commun. 17, 51 (1979).
[13]D. J. Kouri, *Atom Molecule Collision Theory*, edited by R. B. Bernstein (Plenum, New York, 1979), Chap. 9.
[14]R. Goldflam, S. Green, and D. J. Kouri, J. Chem. Phys. 67, 4149 (1977); 67, 5661 (1977).
[15]G. A. Parker and R. T Pack, J. Chem. Phys. 68, 1585 (1978).
[16]G. A. Parker, R. L. Snow, and R. T Pack, J. Chem. Phys. 64, 1668 (1976); R. T Pack, *ibid.* 70, 3424 (1979).
[17]M. Keil, G. A. Parker, and A. Kuppermann, Chem. Phys. Lett. 59, 443 (1978).
[18]R. Schinke and P. McGuire, Chem. Phys. 31, 391 (1978); R. Schinke, *ibid.* 34, 65 (1978).
[19]J. M. Bowman and S. C. Leasure, J. Chem. Phys. 66, 288 (1977).
[20]D. Secrest and C. S. Lin, J. Chem. Phys. 70, 3420 (1979).
[21]J. M. Bowman and S. Leasure, Chem. Phys. Lett. 56, 183 (1978).
[22]D. C. Clary, Mol. Phys. 39, 1295 (1980).
[23]S. Erkoc and J. N. Murrell, Int. J. Quantum Chem. (to be published).
[24]S. Erkoc, J. N. Murrell, and D. C. Clary, Chem. Phys. Lett. 72, 264 (1980).
[25]S. C. Farantos and J. N. Murrell, Int. J. Quantum Chem. (to be published).
[26]G. C. Schatz and M. D. Moser, J. Chem. Phys. 68, 1992 (1978); G. C. Schatz and T. Mulloney, *ibid.* 71, 5257 (1979).
[27]R. L. Thommarson, G. C. Berend, and S. W. Benson, J. Chem. Phys. 54, 1313 (1971).
[28]H. H. Suzukawa Jr., M. Wolfsberg, and D. L. Thompson, J. Chem. Phys. 68, 455 (1978).
[29]N. Sathyamurthy and L. M. Raff, J. Chem. Phys. 66, 2191 (1977).
[30]A. J. Stace and J. N. Murrell, J. Chem. Phys. 68, 3028 (1978).
[31]T. Mulloney and G. C. Schatz, Chem. Phys. 45, 213 (1980).
[32]G. C. Schatz, J. Chem. Phys. 72, 3929 (1980).
[33]G. D. Billing, Chem. Phys. 46, 123 (1980).
[34]H. K. Shin, Chem. Phys. Lett. 2, 629 (1968); 40, 316 (1976).
[35]E. Vilallonga, D. A. Micha, and J. P. Toennies, Chem. Phys. Lett. 68, 352 (1979).
[36]C. H. Chen, P. E. Siska, and Y. T. Lee, J. Chem. Phys. 59, 601 (1973).
[37]C. Y. Ng, Y. T. Lee, and J. A. Barker, J. Chem. Phys. 61, 1996 (1974).
[38]E. B. Wilson, J. C. Decius, and P. C. Cross, *Molecular Vibrations* (McGraw-Hill, New York, 1955).
[39]J. K. G. Watson, Mol. Phys. 19, 465 (1970).
[40]G. Herzberg, *Infrared and Raman Spectra of Polyatomic Molecules* (Van Nostrand, New York, 1945).
[41]D. Secrest, J. Chem. Phys. 62, 710 (1975).
[42]D. M. Brink and G. R. Satchler, *Angular Momentum* (Clarendon, Oxford, 1968).
[43]J. C. Light, J. Ross, and K. E. Shuler, *Kinetic Processes in Gases and Plasmas*, edited by A. R. Hochstim (Academic, New York, 1969), Chap. VIII.
[44]P. J. Davis and I. Polonsky, *Handbook of Mathematical Functions*, edited by M. Abramowitz and I. A. Stegun (Dover, New York, 1965), Chap. 25.
[45]R. J. Whitehead and N. C. Handy, J. Mol. Spectrosc. 55, 356 (1975).
[46]J. C. Light and R. B. Walker, J. Chem. Phys. 65, 4272 (1976); E. B. Stechel, R. B. Walker, and J. C. Light, *ibid.* 69, 3518 (1978).
[47]A. W. Raczkowski, W. A. Lester, and W. H. Miller, J. Chem. Phys. 69, 2692 (1978).
[48]A. R. Edmonds, *Angular Momentum in Quantum Mechanics* (Princeton University, Princeton, N. J., 1957).
[49]M. E. Rose, *Elementary Theory of Angular Momentum* (Wiley, New York, 1957).
[50]K. Kuchitsu and Y. Morino, Bull. Chem. Soc. Jpn. 38, 805 (1965).
[51]P. McGuire and D. J. Kouri, J. Chem. Phys. 60, 2488 (1974).
[52]D. C. Clary, J. Chem. Phys. (to be published).